Metabolic profiling of live cancer tissues using NAD(P)H fluorescence lifetime imaging

Thomas S. Blacker[1,2,3,*], Michael D.E. Sewell[1], Gyorgy Szabadkai[1,2,4,5], Michael R. Duchen[1,2]

[1]Research Department of Cell & Developmental Biology, University College London, Gower Street, London WC1E 6BT, United Kingdom

[2]UCL Consortium for Mitochondrial Research, University College London, Gower Street, London WC1E 6BT, United Kingdom

[3]Department of Physics & Astronomy, University College London, Gower Street, London WC1E 6BT, United Kingdom

[4]The Francis Crick Institute, 1 Midland Road, London NW1 1AT, United Kingdom

[5]Department of Biomedical Sciences, University of Padua, 35131 Padua, Italy

[*]Corresponding Author: t.blacker@ucl.ac.uk

Running Title: FLIM of NAD(P)H

Abstract

Altered metabolism is a hallmark of cancer, both resulting from and driving oncogenesis. The NAD and NADP redox couples play a key role in a large number of the metabolic pathways involved. In their reduced forms, NADH and NADPH, these molecules are intrinsically fluorescent. As the average time for fluorescence to be emitted following excitation by a laser pulse, the fluorescence lifetime, is exquisitely sensitive to changes in the local environment of the fluorophore, imaging the fluorescence lifetime of NADH and NADPH offers the potential for label-free monitoring of metabolic changes inside living tumours. Here, we describe the biological, photophysical and methodological considerations required to establish fluorescence lifetime imaging (FLIM) of NAD(P)H as a routine method for profiling the metabolism of living cancer cells and tissues.

Key words

NADH, NADPH, autofluorescence, fluorescence lifetime imaging, live-cell microscopy, cancer metabolism

1. Introduction

Since the pioneering work of Otto Warburg almost a century ago[1], it has become clear that the metabolic reprogramming of cancer cells is crucial in facilitating their uncontrolled proliferation[2–4]. The "Warburg effect" describes an increase in glucose uptake and lactate generation upon carcinogenesis, despite the presence of abundant oxygen, arising from an apparent switch in the means of producing adenosine-3,5-triphosphate (ATP) from oxidative phosphorylation (OXPHOS) to "aerobic glycolysis". The advantage of this metabolic shift is unclear, given that the complete oxidation of a glucose molecule through OXPHOS yields almost 20 times more ATP than via glycolysis alone[5]. Warburg originally attributed both his observations and the root cause of cancer to defective mitochondria, the organelles at the heart of cell metabolism and the location of the OXPHOS machinery, whose impairment has now been implicated in numerous other pathologies[6]. For many decades, the Warburg effect was presumed to be a biochemical hallmark of all cancers, forming the basis of a widely successful diagnostic tool, positron emission tomography (PET), which measures enhanced radiolabelled glucose uptake to detect tumours[7]. However, later research showed that many tumours and their precursors defy Warburg's hypothesis, predominantly maintaining high ATP/ADP ratios using mitochondrial OXPHOS[8]. Further, subsequent studies have also shown that tumours displaying the Warburg effect still possess functional mitochondria[9–11]. These findings demonstrate a significantly more complex link between cancer and metabolism than in Warburg's initial description. Perhaps unsurprisingly, therefore, a heavy focus on identifying ubiquitous characteristics of neoplastic tumours to develop a "one size fits all" approach to cancer treatment has so far proven unsuccessful, the wide acceptance of the Warburg effect perhaps diverting attention away from the unique metabolic phenotypes of individual cancers[12]. As understanding the pathways active in individual tumours is crucial to developing effective treatment strategies[13], tools for the

metabolic profiling of cancer tissues are vital. This chapter concerns the application of time-resolved measurements of cellular autofluorescence to provide a window into cellular metabolism in cancer, using the intrinsic photophysical properties of the reduced metabolic cofactor nicotinamide adenine dinucleotide (NADH) and its phosphorylated counterpart NADPH.

1.1. The Role of NAD(P) in Cancer

Mitochondria are cytoplasmic organelles that, in normal differentiated cells, act as the primary ATP generator through aerobic respiration[5], in addition to regulating Ca^{2+} signalling, the production of reactive oxygen species (ROS) and cell death[6]. In the presence of oxygen, most differentiated cells catabolise their main fuel, glucose, first through its cytosolic conversion in glycolysis to pyruvate, then by its subsequent transport into the mitochondria and oxidation via the tricarboxylic acid (TCA) cycle[3]. In both mitochondria and cytosol, the electrons removed during this chain of oxidation reactions are passed to NAD+, reducing it to form NADH. The NADH generated by the TCA cycle donates electrons to the electron transport chain (ETC) located on the inner mitochondrial membrane. Glycolytically-derived cytosolic NADH cannot cross the mitochondrial membrane but its reducing equivalents may contribute to this pool by being passed to NAD+ in the mitochondrial matrix via the malate aspartate shuttle[14]. The passage of the electrons donated by NADH along the complexes of the ETC to the terminal electron acceptor, oxygen, is coupled to the pumping of protons from the mitochondrial matrix to the intermembrane space, establishing the membrane potential that powers the production of ATP by ATP synthase. By ferrying electrons from the TCA cycle to the ETC, alongside those removed during glycolysis, NADH plays a pivotal role in linking the oxidation of carbon sources to the storage of the energy liberated in the useable form of ATP.

Disruption of the passage of electrons along the ETC allows electrons to leak directly to O_2, causing its direct reduction to superoxide O_2^-. Such conditions occur in response to hypoxia or upon exposure to respiratory chain inhibitors such as cyanide, and are reflected by an increased NADH/NAD+ ratio[15]. Superoxide acts as the proximal ROS from which other toxic species such as hydrogen peroxide (H_2O_2) can be produced, causing damage inside the cell by reacting directly with proteins, lipids and DNA[14]. The cell contains two thiol-linked antioxidant defence systems to decrease oxidative stress, mediated by glutathione and thioredoxin. Both molecules are maintained in their functional, reduced form by the electron donor NADPH[14]. The phosphate group attached to the adenine end of this NADH analogue allows enzyme binding sites to be distinct to those of its unphosphorylated counterpart. Thus, while the NAD pool participates in ATP yielding catabolic reactions, the NADP pool contributes specifically to anabolic reactions, such as antioxidant maintenance and nucleic acid and fatty acid synthesis[16]. In the mitochondria, the NADPH pool is primarily maintained by the nicotinamide nucleotide transhydrogenase (NNT) which, powered by the mitochondrial membrane potential, reduces NADP+ by oxidising NADH. The NNT thereby siphons a portion of the NADH produced by the TCA cycle to act in an antioxidant capacity as NADPH, defending against oxidative damage caused by the remaining NADH, should electron leak from the ETC occur[14, 17].

The NAD and NADP pools are maintained in vastly different redox balances due to their contrasting intracellular roles. The NADPH/NADP+ ratio is maintained high due to the primary role of the NADP pool in donating electrons to anabolic reactions. In the cytosol this is largely carried out by the pentose phosphate pathway, which may compete with glycolysis for glucose, reducing NADP+ rather than NAD+. Glycolysis itself requires that the NADH/NAD+ ratio is maintained low in the cytosol, as the pathway is unable to proceed if the NAD+ pool is not restored to provide electron acceptors for the key oxidation

reactions[14]. While the malate aspartate shuttle contributes to maintaining this balance, lactate dehydrogenase plays the critical role, converting the end product of glycolysis, pyruvate, into lactate, oxidising NADH to NAD+ in the process. High glycolytic fluxes are therefore necessarily correlated with significant lactate production[18].

The high levels of aerobic glycolysis in cancer cells observed by Warburg occur only under anaerobic conditions in normal cells[3]. Possible reasons for this include a higher ATP production rate compared to OXPHOS[18], or a reduction in ROS generation, excessive quantities of which trigger apoptotic cell death[19, 20]. Cancer cell metabolism is also no longer coupled to oxygen availability according to the Warburg effect, providing a selective advantage within the tumor microenvironment where oxygen concentration is often low or constantly fluctuating due to a disrupted blood supply[21, 22]. Furthermore, glycolytic intermediates may enter the pentose phosphate pathways via the transketolase and transaldolase enzymes, generating NADPH to provide the reducing equivalents required for fatty acid and nucleotide synthesis, in addition to ribose-5-phosphate, forming the backbones of RNA and DNA[14]. Consequently, aerobic glycolysis may fulfil an abundance of the biochemical requirements of a proliferating cell[23]. However, this route to fulfilling the bioenergetic needs of oncogenic proliferation is now known to be but one of many[4].

The metabolic phenotype adopted by a cancer cell is largely dictated by the specific oncogenes and tumour suppressor genes expressed within it, acting on diverse metabolic targets ranging from glucose metabolism and substrate transport to redox homeostasis and protein, lipid and nucleic acid synthesis[4, 24, 25]. p53 deficient tumours have been shown to be particularly reliant on serine metabolism, feeding into the folate and methionine cycles for the reactions involved in one carbon metabolism[26]. This has led to the emergence of serine starvation as a particularly attractive therapeutic target[27]. The importance of glutamine to cancers, feeding directly into the TCA cycle by its conversion into α-ketoglutarate via

glutamate, has long been known and appears to be regulated by the c-MYC oncogene[28]. Additionally, metabolism may not only act to provide the energy and building blocks required for proliferation but may also generate products that directly cause oncogenic transformation, so-called "oncometabolites"; a mutation in the enzyme isocitrate dehydrogenase creates a mutant form that can convert α-ketoglutarate into 2-hydroxyglutarate (2-HG), the accumulation of which hampers differentiation[29]. These examples show that the 21st century "post Warburg" understanding of the links between cancer and metabolism is one of a panoply of potential routes by which metabolism can both drive and support tumorigenesis[4].

Importantly for the techniques described in this chapter, the majority of the metabolic pathways commandeered by a cancer cell to ensure its proliferation are dependent on redox reactions in which the NAD and NADP pools participate, as summarised in Figure 1. In addition to the well known roles of these cofactors in the glycolytic and OXPHOS pathways perturbed by the Warburg effect, serine biosynthesis involves the reduction of NAD+ to NADH, the conversion of glutamine to α-ketoglutarate involves the reduction of NADP+ to NADPH and the production of 2-HG by mutant isocitrate dehydrogenase relies on reversing its normal function from an NADP+ reducing to an NADPH oxidising form[27–29]. The NAD and NADP pools therefore lie at the heart of the complex web of links between cancer and metabolism and, as such, their biochemical status may offer insight into the specific metabolic pathways active in a given tumour. The development and application of such approaches is made all the more appealing as the reduced cofactors can be observed in living tissues using laser scanning microscopy without the need for the addition of extrinsic dyes[14].

1.2. Autofluorescence of NADH and NADPH

The reduction of NAD+ to NADH involves the transfer of a hydride ion to its nicotinamide ring. This decreases the energy gap between the highest occupied molecular orbital (HOMO) and the lowest unoccupied molecular orbital (LUMO) of the moiety by approximately 2 eV, shifting the wavelength of light at which it maximally absorbs from the far-ultraviolet 220 nm to the near-visible 340 nm[30]. As a complex molecule, the large number of vibrational degrees of freedom available in NADH broadens its absorption spectrum by around 30 nm on either side of this peak. Absorption of light at these wavelengths causes a transition into an excited electronic state. In aqueous solution at room temperature, the fate of 98% of the absorption events is to cause small scale motion of the nicotinamide ring[31]. However, the remaining 2% of the photons absorbed are reemitted as fluorescence. Excess vibrational energy dissipated to the surroundings following excitation causes the fluorescence photons to carry less energy than those absorbed. NADH therefore emits light of wavelength 460(±25) nm[32].

The intrinsic fluorescence of NADH has been used as a reporter of metabolic state since the pioneering experiments of Britton Chance in the 1950's[33]. Chance used changes in the fluorescence emitted from living tissues following illumination at 366 nm to monitor changes in the redox state of the NAD pool, and thus interrogate the function of the ETC in intact tissues for the first time[34]. Our lab routinely uses a modern adaptation of these experiments to estimate the redox state of the mitochondria in live cell models[35]. In a confocal microscope with 351 nm excitation and 435-485nm emission filtering, the resting NADH fluorescence level is compared with maximally oxidised and maximally reduced conditions. These are achieved respectively by application of the uncoupler carbonyl cyanide-p-trifluoromethoxyphenylhydrazone (FCCP), causing complex I of the ETC to oxidise NADH at its maximum rate, and cyanide, inhibiting the ETC and thus terminating NADH oxidation.

However, a caveat to this method is in its assumption that NADH is the only fluorescent molecule present in this spectral region that may respond to these pharmacological perturbations. The contribution from NADPH is neglected[14].

As the phosphate group which allows enzymes to distinguish between the NADP and NAD pools lies at the adenine end of the molecule, far from the redox-active and fluorescent nicotinamide ring, NADH and NADPH are spectrally identical[32]. Conventional, intensity based fluorescence measurements can therefore not distinguish between these two dinucleotide pools, leading to the labelling of their combined signal as NAD(P)H[14, 35]. However, such a technique would be desirable, given the drastically different elements of intracellular metabolism that the NAD and NADP pools are involved in regulating. We recently addressed this issue by applying fluorescence lifetime imaging microscopy (FLIM). The fluorescence lifetime of a molecule measures the average amount of time it spends in the excited state following absorption. Addition or removal of the pathways available for a molecule to leave the excited state will therefore alter the fluorescence lifetime[36]. Enzyme binding is known to restrict the small scale motions that account for a large majority of the deexcitation events occurring in NADH[37], thereby decreasing the rate at which the molecules leave the excited state, increasing the fluorescence lifetime. Concomitantly, a greater proportion of excitation events in enzyme bound NADH will result in fluorescence compared to free NADH in solution, increasing its brightness. In solution, NADH and NADPH share a fluorescence lifetime of approximately 0.4 ns[31]. Our work suggested that, inside live cells, the binding site of NADPH increases its fluorescence lifetime to a greater extent than that of NADH, at around 4.4 ns to 1.5 ns[38]. Combining NAD(P)H imaging with FLIM thereby allows the relative contributions of NADH and NADPH to the total signal to be determined, allowing NAD and NADP associated pathways to be separately interrogated in living tissues for the first time.

1.3. Studying Cancer Metabolism using NAD(P)H FLIM

Time-resolved measurements of NAD(P)H fluorescence in living biological samples were first performed over 25 years ago[39] when Schneckenburger and Koenig showed, in live yeast cells, that the fluorescence lifetime of NAD(P)H was increased relative to its lifetime free in solution, indicative of enzyme binding. In subsequent work[40], again in yeast, Paul and Schneckenburger demonstrated a correlation between oxygen tension and the average lifetime of the NAD(P)H signal. With the Warburg hypothesis in place for 70 years, this finding inevitably motivated the initial comparisons of the time-resolved fluorescence properties of NAD(P)H in cancers relative to healthy tissue. Pradhan and colleagues compared the fluorescence lifetime of NAD(P)H in metastatic and non-metastatic variants of a number of cancer cell lines in suspension[41]. The average lifetime was approximately three-fold lower in metastatic cell lines relative to their non-metastatic counterparts. The potential for time-resolved NAD(P)H fluorescence measurements to act as a label-free "Warburg sensor" was thus established.

As discussed in section 1.1, the Warburg effect is not a universal feature of all cancers; carcinogenesis is critically dependent on a wide range of metabolic shifts[4]. Given that a number of these cause alterations in the redox balance of the NAD and NADP pools, and that fluorescence lifetime measurements are sensitive to the balance between the reduced forms of these two nucleotides[38], NAD(P)H FLIM measurements can be used as a direct reporter of metabolic differences between cancer tissues. The commercialisation of time-resolved imaging add-ons to laser scanning microscope systems in the early 2000's has allowed the number of studies reporting differences in the fluorescence decay of NAD(P)H between healthy and cancer tissues to increase steadily from 2005 onwards (Figure 2). In this year, a now highly cited study by Bird and co-workers demonstrated the sensitivity of the NAD(P)H fluorescence lifetime to metabolic perturbation in breast epithelial cells, raising hope of an

11

optical technique for staging breast tumours[42]. Correlations between the fluorescence lifetime and cancer stage were subsequently observed in a hamster cheek model of oral carcinogenesis[43]. In 2010, McGinty et al. demonstrated a widefield instrument able to delineate the boundaries of colonic adenocarcinoma using time-resolved measurements of tissue autofluorescence[44]. Adur et al. have since shown that a significant increase in the average NAD(P)H lifetime inside the tumour contributes to this capability[45]. Longer average NAD(P)H fluorescence lifetimes have also been observed in malignant oral mucosa cell lines compared to their non-malignant counterparts[46] and in cancerous, relative to non-transformed, cervical tissues[47]. In contrast, Skala et al. showed *in vivo* that the fluorescence lifetime of NAD(P)H in healthy oral epithelial cells is longer than in the neighbouring precancerous tissue[43]. Shorter average lifetimes were also observed in cancerous cell lines relative to control by Awasthi et al.[48], and in melanomas relative to healthy skin by Pastore et al.[49]. The complex changes in metabolism during carcinogenesis are therefore reflected in complex variations in NAD(P)H lifetimes. Nevertheless, FLIM of NAD(P)H has now established itself as a robust and reliable method for detecting metabolic shifts in cancers.

The majority of the studies discussed here, alongside those in the literature, are based on the time correlated single photon counting (TCSPC) technique. The principles of this method are outlined in Figure 3. Its practical application for the study of metabolic shifts in cancers is the subject of the remainder of this chapter.

2. Materials

2.1. Pulsed laser source

A pulsed excitation source is a key feature of the TCSPC technique and represents an important difference between fluorescence lifetime and routine confocal imaging[50]. Many well equipped microscopy facilities will now offer two-photon imaging platforms, which rely on the use of a pulsed laser operating in the red to near-infrared portion of the spectrum to excite the target molecule using the near-simultaneous arrival of two photons each carrying half the energy of the single photon transition[51]. Consequently, FLIM electronics can be added directly to these existing systems without the requirement for a new dedicated laser. The widely tuneable Ti:sapphire laser has become the workhorse instrument for such applications, providing short (~100 fs) pulses operating at ~80 MHz repetition rates[52]. This ensures that there is sufficient delay between excitation pulses (~10 ns) to measure the NAD(P)H fluorescence decay, with more than 99% of the initial excited state population having decayed by the time the next pulse arrives. Two-photon excitation provides a means by which to achieve increased depth penetration into complex biological tissue preparations[53], making it a popular choice for clinical application of NAD(P)H FLIM. However, NAD(P)H FLIM with single photon excitation has previously been applied[54], offering the advantage of increasing the signal at the expense of axial resolution by opening the confocal pinhole[55]. A number of excitation laser solutions could be applied for this purpose. Single wavelength diode-pumped solid state (DPSS) lasers with <100ps pulse widths are becoming available operating at the appropriate wavelength for single photon excitation at ~340nm, the output of a Ti:sapphire laser can be frequency doubled using an appropriate crystal (e.g. lithium triborate) or an optical parametric oscillator system can be used to extend the tuning range of the Ti:sapphire into the visible.

2.2. Laser scanning microscope

The pulsed laser excitation source must be coupled to a laser scanning confocal microscope equipped with an objective lens of suitable magnification for the biological preparation to be studied. An appropriate selection of dichroic mirrors and emission filters must also be available. Short-pass dichroic mirrors are required for two-photon excitation as the fluorescence emission results at a shorter wavelength than the incident illumination. The excitation conditions used for NAD(P)H may also cause absorption in a number of other intrinsic fluorophores, particularly flavins which emit at longer wavelengths around 530(±30)nm[38]. Emission filters specific for NAD(P)H should therefore be used, such as a band pass around the emission peak at 460nm. FLIM relies on performing the TCSPC technique at each pixel of the image, so the microscope must also provide scan signal outputs for the pixel registration of the detected photons and allow the attachment of an external detector (see section 2.5).

2.3. Sample mounting considerations

Maintaining the biological integrity of the sample of interest at the microscope is a vital aspect of the imaging process. The sample must be kept sufficiently still over the time required to acquire sufficient photons to generate a FLIM image (of the order of minutes, see section 5.3) so as to not cause spatial blurring in the resulting dataset. The choice of buffer solutions, perfusion systems and environmentally-controlled chambers to maintain the physiological integrity of the living sample will vary from preparation to preparation, and determining the correct conditions is likely to be a significant undertaking at the start of a new research project. However, live cell and tissue imaging is now a sufficiently mature field that commercial solutions to a range of sample mounting issues are available, allowing NAD(P)H FLIM studies to be performed on a diverse array of biological samples, from cell cultures on coverslips to *in vivo* tumours.

2.4. TCSPC detector

The internal detectors of the microscope are unlikely to provide the single photon sensitivity required to perform the TCSPC technique. As such, an external detector must be attached to the microscope at a suitable exit port. Microscope systems designed for multiphoton imaging should provide non-descanned ports for this purpose. As two-photon excitation does not require the use of a confocal pinhole, the path followed by fluorescence to exit a non-descanned port should contain fewer optical elements, increasing the detection efficiency and ultimately the sensitivity of the technique[56]. The most frequently used detectors for TCSPC applications are photomultiplier tubes (PMTs)[57]. Here, a single photon causes the ejection of electrons from a photocathode which, via acceleration through an electric field and subsequent collisions with further dynodes, cause a detectable current pulse at the anode. The use of a hybrid PMT should be considered for studies involving NAD(P)H fluorescence lifetimes[58]. These detectors remove a large number of the signal amplification steps, instead accelerating photoelectrons directly into a semiconductor diode. This shortens its time resolution by almost an order of magnitude from the hundreds of picoseconds for a conventional PMT, close to the fast lifetime of free NAD(P)H, increasing the accuracy with which the fluorescence decay parameters can be determined. The extreme sensitivity of these detectors makes them highly susceptible to damage from leakage of ambient light, so a shutter assembly with automatic overload sensing is crucial.

2.5. TCSPC electronics

While the earliest implementations of the TCSPC technique were modular pieces of electronic laboratory apparatus, modern applications make use of miniaturised circuitry such that all the components can be condensed onto a hardware card inside a desktop PC[59]. Counting cards are available commercially from Becker and Hickl and PicoQuant, amongst others. These companies are also the preferred source of bespoke detectors and shutter

assemblies optimised to both their photon counting electronics and the microscope upon which it is to be mounted. The cards will register the detection of photons and measure the time delay between the laser pulse and emission (see Figure 3), ascribing the event to the appropriate pixel using the signals provided by the microscope scanner. The hardware will interface with appropriate acquisition software to control the relevant experimental parameters, such as collection time, and allow the data to be saved for subsequent analysis.

2.6. Operation and Analysis PC

The fast rate of detected emission events induced by a MHz excitation pulse train prompts the recommendation of a dedicated PC for control of the FLIM acquisition, with background software kept to a minimum to avoid buffer overflows and data corruption. The resulting image files contain count data for hundreds of channels in each of tens of thousands of pixels so the resulting images can be large (10-100 MB per image). As such, access to high-volume (~TB) external storage is important for multi-user facilities. Such facilities should also consider dedicated analysis computers for extracting fluorescence decay parameters from TCSPC data as pixel-by-pixel curve fitting approaches (see section 4) can be time-consuming. The more powerful these machines, the faster the fitting and subsequent analysis can take place.

3. Methods

1. Tune the laser to the appropriate wavelength. For single-photon studies, this should be as close to the absorption peak at 340nm as possible. With two-photon excitation, NAD(P)H maximally absorbs at 700 nm[60]. However, this is close to the minimum wavelength achievable using a Ti:sapphire laser and many models may be unable to maintain a stable, modelocked output. In such situations, a wavelength as close to 700 nm as possible should be used, in order to maximise the proportion of NAD(P)H excited relative to other intrinsic fluorophores that may absorb in this spectral range[60]. The incident power should be chosen in accordance with the considerations discussed in section 5.2.

2. Select a dichroic mirror appropriate to the excitation conditions used. This optical component allows the incident illumination to be separated from the spectrally-shifted fluorescence. The mirror should reflect the excitation wavelength onto the sample through the objective, allowing the fluorescence to be transmitted through it to the detectors. For single photon excitation, the dichroic should transmit light of longer wavelength than that absorbed by the NAD(P)H. Dichroic mirrors for two-photon must transmit light of a shorter wavelength than that reflected.

3. Select emission filters appropriate for isolating the NAD(P)H signal. A bandpass filter centred on the emission peak at 460nm is recommended. Whilst this cannot guarantee exclusion of all autofluorescent compounds that absorb in this spectral region, we have previously estimated that use of a 460(±25)nm emission filter with excitation between 700 nm and 740 nm is 95% specific for NAD(P)H[38].

4. Locate the sample in the microscope eyepieces using brightfield illumination and roughly bring it into focus. Start a fast scan and use the internal detectors of the microscope to observe the NAD(P)H fluorescence from the sample. Fine-tune the

focus to observe the desired focal plane and translate the image until the required region is located. Rotate and crop the image as necessary, remembering that increased zoom may reduce the signal levels obtainable due to the increased likelihood of photodamage.

5. Adjust the microscope settings to send the NAD(P)H signal to the external detector connected to the TCSPC system. Begin a fast scan and acquire a FLIM image for a predetermined length of time, chosen based on the considerations discussed in section 5.3.

6. Repeat the imaging process across different regions of the same sample, if possible, and across biological replicates for each experimental condition. Guidance for choosing a suitable number of repeats is given in section 5.5.

4. Data Analysis

The data produced by a traditional TCSPC experiment performed on a fluorophore solution in a cuvette consist of the number of photons emitted by the solution as a function of time after excitation by a laser pulse. Time-resolved fluorescence microscopy extends this into two spatial dimensions, obtaining these decay measurements at every pixel of an image. A FLIM image is therefore a significantly more complex entity than a standard intensity-based fluorescence image, the analysis of which can subsequently be more involved. Here, the principle means by which to derive metabolic information from the data contained within an NAD(P)H FLIM image are discussed.

4.1. Bi-exponential fitting

NADH and NADPH may bind to a vast array of different enzymes inside the cell, all of which may induce slightly different fluorescence lifetimes[14]. The cofactors may also exist in an unbound form, exhibiting a correspondingly shorter lifetime[31]. Each pixel of an NAD(P)H FLIM image could therefore be expected to contain a highly heterogeneous mix of different fluorescent species with different fluorescent lifetimes. In such a circumstance, multiexponential fitting can be employed. This method is generally available in the software provided by commercial vendors of FLIM systems, such as Becker & Hickl's SPCImage and PicoQuant's Fluofit. A fitting algorithm varies the lifetimes and weightings of a sum of exponential decays until a good fit is achieved between model and data[61]. The relative weightings of each decay component then represent the relative abundances of each fluorescent species. However, as fluorescence emission is a stochastic process, Poisson noise inherent in the fluorescence decay reduces the ability to separate the contributions of every species to the measured signal[38]. The signal to noise ratio of such a process increases as the square root of the signal[62], however at the signal levels obtainable in live tissues, only two components can be reliably resolved[38]. A basic rule of thumb states that ten times more

19

signal is required to resolve every additional component[63]. Observing even a third component would therefore require a ten-fold increase in the acquisition time of each image to 10 minutes or more, rendering the technique impractical and increasing the risk of phototoxicity[64]. Fortunately, the two lifetimes extracted have been shown to represent average values of the free and enzyme-bound species present, τ_{free} and τ_{bound}[38]. Their relative weighting α_{bound} therefore provides the percentage of total NAD(P)H that is enzyme-bound at a given pixel.

4.2. Statistical fitting methods

Biexponential analysis using weighted least-squares curve fitting is the most commonly employed method for extracting the NAD(P)H fluorescence decay parameters from the acquired FLIM data[14]. The method relies on minimisation of the χ_R^2 fitting statistic, which compares the magnitude of deviations between the proposed model and the experimental data relative to the differences expected purely from the presence of Poisson noise[65]. If the difference between the data and the model is larger than that expected from the noise, χ_R^2 is large. If the only differences between the model and the data can be ascribed to Poisson noise, χ_R^2 is approximately 1. The software fitting algorithm acts by varying the model parameters until χ_R^2 is minimised. In conditions of low signal, such as may be encountered in cells with low NADH and NADPH levels or with high susceptibility to phototoxicity, the statistical assumptions of the least-square fitting process can break down[66] and the lifetimes become biased towards incorrect values[67]. This can be corrected by making use of a maximum likelihood estimator for the fitting statistic, which aims to find the fluorescence decay parameter values that maximise the statistical likelihood of obtaining the measured dataset[68, 69]. This approach is available in the OMERO FLIMfit software[70]. By recasting the problem as the recovery of a probability distribution of lifetimes present in the

data, it is also possible to apply the maximum entropy method to further refine the correct extraction of fluorescence decay parameters[71, 72], however this approach has, to the best of our knowledge, yet to be applied to FLIM. One potentially powerful advanced statistical method which has been successfully applied to time-resolved fluorescence imaging is the "fit free" approach of Bayesian inference[73, 74]. Here, the arrival times of each photon in turn are used to update the likelihood of a given underlying set of decay parameters. The method has been shown to give significantly more precise estimates of fluorescence lifetimes and decay amplitudes for measurements up to 10000 photons, similar to that which may be obtained in an NAD(P)H FLIM image with acquisition times of the order of minutes[73].

4.3. Phasor analysis

The enhanced-precision analysis approaches described above will play an important role in the application of FLIM as a precise, quantitative experimental technique, providing absolute, numerical information to aid the ongoing goal of a predictive, model-based 21st century biology[75]. However, to date, NAD(P)H FLIM has largely been applied as a qualitative and descriptive tool in which changes in the fluorescence decay parameters are used to infer alterations in the metabolic state of a tissue. User-friendliness and minimised data processing times are therefore a priority in the choice of analysis method. Over the last decade, phasor analysis of NAD(P)H FLIM data has become a popular means by which to fulfil these criteria, generally using the Globals software (Laboratory for Fluorescence Dynamics, Irvine, USA)[76]. The method involves using the real and imaginary components of the Fourier transform of the TCSPC data at each pixel of the FLIM image as coordinates of points in a two-dimensional phase space known as the phasor plot. Each pixel in the FLIM image will correspond to a location in the phasor plot, the coordinates of which reflect the shape of the fluorescence decay at that pixel. Pixels with similar fluorescence decay characteristics will cluster around similar locations in the phasor plot, providing a graphical means by which to

deduce heterogeneity within the fluorescence lifetimes present across an image[76]. Changes in the relative abundance of two or more species can also be graphically inferred; pure solutions of freely diffusing and enzyme bound NAD(P)H will occupy specific points in the phasor plot, and changing the proportion of free and bound NAD(P)H in a mixture of the two species will move the coordinates of its fluorescence decay along the straight line joining the two primary points. As the phasor approach does not require fitting of the fluorescence decay data, it is computationally simple and therefore fast. For this reason, its implementation has contributed significantly to the growth in applications of NAD(P)H fluorescence lifetime imaging in recent years[77–79].

5. Notes

5.1. Instrument response function measurement

The TCSPC components of a FLIM system do not operate infinitely fast. In fact, a distribution of lag times may exist between arrival of a fluorescence photon at the detector and registration of an emission event in the control PC. This distribution, the instrument response function (IRF), has a width which is typically of the order of 100ps, close to the time scale over which fluorescence from free NAD(P)H decays; its influence must therefore be taken into account. Most FLIM analysis software provides the functionality to deconvolve the effect of the IRF in the extraction of fluorescence decay parameters. The user must provide it with a measurement of the fluorescence decay of a sample with infinitely short fluorescence lifetime, such as a scattering solution for single photon measurements or second harmonic generation from a collagen sample for two-photon systems. Unfortunately both methods are technically inadequate as the measured signal in this calibration will not be at the wavelength of the fluorescence to be observed in the final experiment. One solution is to use a gold nanorod solution as a target, which has been shown to have a wide emission profile as well as the required negligible lifetime[80].

5.2. Laser power choice

Increased excitation power will increase the amount of fluorescence emitted, reducing the influence of Poisson noise on the measurements and therefore allowing fluorescence decay parameters to be determined with increased accuracy. Additionally, increased signal will allow the amount of pixel binning to be reduced (see section 5.4), increasing the spatial resolution of the FLIM image. However, laser power cannot be increased without limit, as photodamage will begin to reduce the biological viability of the sample under study. 98% of the energy absorbed by free NAD(P)H is converted into heat[31]. Laser light can also directly

induce the direct oxidation of NADH and the subsequent production of free radicals[81]. As such, NAD(P)H photobleaching is typically used as a proxy for the onset of photodamage[38, 82]. The ideal laser power can then be chosen as the highest value that does not cause photobleaching over the acquisition period. Laser repetition rate and pulse width will affect the incident photon flux and would thus likely be a factor in the level of photodamage at a given average excitation power[83]. However, these properties of the incident beam are difficult to control in a user-friendly microscope set-up. Instead, the scan speed and zoom level can be adjusted to limit laser dwell times. For extra confidence in the chosen settings, short bursts of data can be collected at the start and end of an image acquisition and the data obtained can be binned into two single decays[38]. If the NAD(P)H fluorescence decay parameters are the same in the two decays, the user can be assured that the laser has not caused significant perturbation to the metabolism of the sample under study.

5.3. Acquisition time considerations

The maximum rate at which photons can be detected in a TCSPC experiment is limited to 1% of the incident laser repetition rate[84]. This rule of thumb reduces to insignificance the likelihood of more than one photon arriving in the time delay between two pulses. Based on a computational analysis of the signal-dependent uncertainty in the parameters obtained from biexponential fitting[38], we typically aim to acquire sufficient fluorescence to register at least 200 counts in the peak of each decay in the image. Acquiring at the maximum rate using an 80MHz Ti:sapphire laser, assuming a homogeneous distribution of emission events across a 256x256 FLIM image and 256 detection channels, the peak value is given by $I(t=0) \approx 40T$ for typical NAD(P)H fluorescence decay characteristics ($\alpha_{\text{bound}} = 0.2$, $\tau_{\text{free}} = 0.4\,\text{ns}$, $\tau_{\text{bound}} = 2.5\,\text{ns}$), where T is the acquisition time in minutes. Each image must therefore be acquired for around 5 minutes to detect sufficient signal. Unfortunately, the requirement to keep incident laser powers low enough to avoid photobleaching means

fluorescence count rates can be significantly less than the maximum rate permitted by the equipment. Indeed, 5×10^4 counts per second are typical in our hands, 16 times below the pulse pileup threshold. Obtaining an image over 80 minutes is wholly impractical; living samples will move and perhaps alter their metabolism over this timescale. It is therefore not possible to acquire sufficient counts at each pixel for a reliable analysis based on increased acquisition times alone, and signal must be increased by other means, notably spatial binning (see section 5.4). Meanwhile, a practical acquisition time should be chosen. This should be long enough to allow the spatial resolution of relevant features of the sample that may be analysed separately, for example subcellular organelles such as the nucleus or mitochondria, or different cell types in a complex tissue. The acquisition time must also be short enough such that the biological integrity of the sample is maintained, both during the collection of an individual image while the sample is exposed to the laser and over the longer time period that the sample remains at the microscope while repeats are being taken in different regions of the preparation. Acquisition times of between 1 and 5 minutes are typical[38, 43, 85].

5.4. Spatial binning

The impracticality of acquiring sufficient counts at an individual pixel for reliable fitting to NAD(P)H FLIM data means that spatial binning of the collected photons is required. This procedure, typically performed by the FLIM analysis software, will combine detection events from surrounding pixels at each location of the image in order to increase signal levels and decrease the relative impact of noise on the uncertainty in the reported parameters. Typically, we will increase the binning level until 200 counts are in the peak channel of the lowest intensity pixel of interest[38]. The extent to which the data are binned is frequently reported as the "binning factor". A binning factor of 1 indicates that the data from the 8 surrounding pixels are added to that in each pixel, resulting in a 9-fold increase in signal, at the expense of spatial resolution. As Poisson statistics apply, this can be expected to decrease the uncertainty

in the fit parameters by a factor of approximately $1/\sqrt{9}$, or to 33% of their initial value. Increasing the binning further to include the 5x5 region surrounding each pixel, a binning factor of 2, will reduce the uncertainties to $1/\sqrt{25}$ of their single-pixel value, a further improvement of 13% over the first level of binning. The gains in parameter precision by additional binning steps then diminish significantly, to 6%, 3% and 2% by increasing to binning factors of 3, 4 and 5 respectively. There is therefore little benefit to applying a binning factor above 2 should the threshold of 200 peak photon counts not be reached, with increases merely reducing the spatial resolution of the FLIM image. Increased certainty in the parameters determined can instead be achieved by taking averages across regions of interest of single measurements, and across repeat measurements of identical conditions.

5.5. Averaging and repeats

A FLIM image of a homogeneous solution of a fluorescent dye with a single lifetime will still report pixel-to-pixel variations in the measured fluorescence decay rate due to the Poisson noise inherent in the TCSPC method. Interpreting these noise-induced variations as physical phenomena can lead to extreme conclusions regarding intracellular heterogeneity of biological properties, such as in the use of temperature-sensitive lifetime probes[86]. The effect of this noise can be eliminated by taking average parameter values across pixels. This can be performed by exporting lifetime images from the lifetime analysis package for analysis in ImageJ (National Institutes of Health, Bethesda, USA). Performing this procedure implies the underlying assumption that the local environment of the fluorescent probe at each pixel is the same. Inside the complex environment of the cell, this assumption does not hold. In the case of NAD(P)H, three distinct microenvironments can be resolved from the fluorescence intensity image itself; the cytosol, the darker nucleus and the brighter mitochondria. As such, we typically extract cytosolic-, nuclear- and mitochondrial-specific

NAD(P)H fluorescence decay parameters from each image we acquire. The mean NAD(P)H lifetime is typically shorter in the nucleus than the rest of the cell. We have shown this to be consistent with equal NADH levels but decreased NADPH levels in the nucleus of HEK293 cells[38]. Despite differing total NAD(P)H concentrations, the mitochondria and cytosol typically display similar fluorescence decay parameters, likely reflecting the high interconnectivity of the redox states of the NAD and NADP pools within and between these two compartments[14, 16, 87]. As with all measurements on living systems, these single region-of-interest measurements are not sufficient to support hypotheses due to the need to account for biological variability. Replicate measurements on independent samples must therefore be taken. We typically observe standard deviations in the fluorescence decay parameters of around 3%. Based on statistical power analysis, around 8 biological replicates would be required for a difference in lifetime of the order of the IRF width (~100 ps) to be reported with a P value of less than 5% in 90% of experiments. This reduces to 3 repeats for reporting statistically significant differences of the order of two IRF widths (~200 ps). The oft-quoted "n=3" should therefore be modestly exceeded in order to make inferences that exploit the full time resolution of the TCSPC method.

5.6. Experimental design summary

The above considerations point to the initial steps of designing an NAD(P)H FLIM experimental protocol outlined below. The procedure can then be tailored to the biological model under investigation as required.

- Choose an acquisition time of between 1 and 5 minutes. Longer times are preferable but the preparation must remain still and viable over the imaging time course.
- Choose the highest laser power that doesn't cause photobleaching over the acquisition time.

- Aim to perform more than 3 independent biological repeats of each condition to ensure that the smallest technically-feasible differences in lifetime can be reliably determined.

- In the analysis stage, increase binning to a maximum of two. Lower binning is better, but aim for the dimmest pixels of interest to contain at least 200 photons counts in the peak channel.

- Separately extract mean NAD(P)H fluorescence decay parameters from the cytosol, nucleus and mitochondria. Organelle-specific dyes (e.g. TMRM) could be used to facilitate this process if the compartments cannot be resolved by the NAD(P)H intensity alone.

6. Conclusions

The original applications of NAD(P)H FLIM in live cells and tissues were content to identify changes in the fluorescence decay characteristics of the signal as indicators of unspecified metabolic alterations. The contemporary ambition is to derive true biological understanding from intracellular NAD(P)H lifetime data by translating fluorescence decay parameters into underlying biochemical and physiological states[14]. With the Warburg effect in mind, the large number of demonstrations of altered autofluorescence lifetimes in cancer relative to healthy tissue prompted developments in this area to focus on the effect of alterations in the balance between aerobic and anaerobic energy metabolism on the NAD(P)H fluorescence decay characteristics[43].

The application of pharmacological perturbations to alter the balance in ATP production between OXPHOS and glycolysis in a given cell type have been observed to correlate with changes in the proportion of bound NAD(P)H species, α_{bound}[42]. However, these correlations may not hold for the comparison of metabolic states in two independent cells or tissues[88]. Indeed, we have previously shown that a genetically modified HEK293 cell line with increased reliance on OXPHOS exhibits the same NAD(P)H fluorescence decay characteristics as the more glycolytic wild-type cells[38]. In addition, a differently modified HEK293 cell line with identical aerobic/anaerobic respiratory balance showed vastly different NAD(P)H fluorescence decay characteristics. The modifications in question were under- and over-expression of NAD kinase, the master regulator of NADPH levels inside the cell. These results demonstrated that the NADPH/NADH balance plays a crucial role in determining the time-resolved NAD(P)H fluorescence characteristics from a given tissue, and that correlations between the bound weighting and the means of ATP production may only apply to acute, externally-induced changes and may not be an overall feature of the metabolic phenotype.

Deciphering the biochemical and physiological meaning behind alterations in the subcellular photophysics of NADH and NADPH remains an active and developing area of research[89]. Nevertheless, exploiting the high sensitivity of fluorescence lifetime measurements to metabolically-induced alterations in the local environment of intrinsic fluorophores continues to be applied as a robust, precise and minimally-invasive means to detect changes in the metabolism of living cells and tissues. Medical devices based on these phenomena for monitoring cancer progression and delineating the boundaries of surgically-accessible tumours are being constructed[90–92]. The extent to which these developments succeed clinically is reliant on integrating fundamental scientific understanding across scales and disciplines, from excited state decay processes and mitochondrial redox dynamics to statistical analysis of single photon counting data and metabolic coupling between cells in a complex tissue, positioning NAD(P)H FLIM as a clear demonstration of the integrative frontiers of modern biomedical research.

References

1. Koppenol WH, Bounds PL, Dang C V (2011) Otto Warburg's contributions to current concepts of cancer metabolism. Nat Rev Cancer 11:325

2. Kim J, Dang C V (2006) Cancer's molecular sweet tooth and the Warburg effect. Cancer Res 66:8927–8930

3. Vander Heiden MG, Cantley LC, Thompson CB (2009) Understanding the Warburg Effect: The Metabolic Requirements of Cell Proliferation. Science (80-) 324:1029–1033

4. Vander Heiden MG, DeBerardinis RJ (2017) Understanding the intersections between metabolism and cancer biology. Cell 168:657–669

5. Osellame LD, Blacker TS, Duchen MR (2012) Cellular and molecular mechanisms of mitochondrial function. Best Pract Res Clin Endocrinol Metab 26:711–723

6. Duchen MR, Szabadkai G (2010) Roles of mitochondria in human disease. Essays Biochem 47:115–137

7. Gambhir SS (2002) Molecular imaging of cancer with positron emission tomography. Nat Rev Cancer 2:683

8. Wallace DC (2012) Mitochondria and cancer. Nat Rev Cancer 12:685–98

9. Weinhouse S (1976) The Warburg hypothesis fifty years later. Zeitschrift für Krebsforsch und Klin Onkol 87:115–126

10. Fantin VR, St-Pierre J, Leder P (2006) Attenuation of LDH-A expression uncovers a link between glycolysis, mitochondrial physiology, and tumor maintenance. Cancer Cell 9:425–434

11. Moreno-Sánchez R, Rodríguez-Enríquez S, Marín-Hernández A, Saavedra E (2007) Energy metabolism in tumor cells. FEBS J 274:1393–1418

12. Robertson-Tessi M, Gillies RJ, Gatenby RA, Anderson ARA (2015) Impact of metabolic heterogeneity on tumor growth, invasion, and treatment outcomes. Cancer Res 75:1567–1579

13. Granger A, Mott R, Emambokus N (2016) Hacking Cancer Metabolism. Cell Metab 24:643–644

14. Blacker TS, Duchen MR (2016) Investigating mitochondrial redox state using NADH and NADPH autofluorescence. Free Radic Biol Med 100:

15. Murphy MP (2009) How mitochondria produce reactive oxygen species. Biochem J 417:1–13

16. Ying W (2008) NAD+/NADH and NADP+/NADPH in cellular functions and cell death: regulation and biological consequences. Antioxid Redox Signal 10:179–206

17. Nickel AG, von Hardenberg A, Hohl M, et al (2015) Reversal of Mitochondrial Transhydrogenase Causes Oxidative Stress in Heart Failure. Cell Metab 22:472–84

18. DeBerardinis RJ, Lum JJ, Hatzivassiliou G, Thompson CB (2008) The biology of cancer: metabolic reprogramming fuels cell growth and proliferation. Cell Metab 7:11–20

19. Sosa V, Moliné T, Somoza R, et al (2013) Oxidative stress and cancer: an overview. Ageing Res Rev 12:376–390

20. Tomiyama A, Serizawa S, Tachibana K, et al (2006) Critical role for mitochondrial oxidative phosphorylation in the activation of tumor suppressors Bax and Bak. J Natl Cancer Inst 98:1462–1473

21. Kroemer G, Pouyssegur J (2008) Tumor cell metabolism: cancer's Achilles' heel. Cancer Cell 13:472–482

22. Hsu PP, Sabatini DM (2008) Cancer cell metabolism: Warburg and beyond. Cell 134:703–707

23. Shlomi T, Benyamini T, Gottlieb E, et al (2011) Genome-scale metabolic modeling elucidates the role of proliferative adaptation in causing the Warburg effect. PLoS Comput Biol 7:e1002018

24. Croce CM (2008) Oncogenes and cancer. N Engl J Med 358:502–511

25. Levine AJ, Puzio-Kuter AM (2010) The control of the metabolic switch in cancers by oncogenes and tumor suppressor genes. Science (80-) 330:1340–1344

26. Locasale JW (2013) Serine, glycine and one-carbon units: cancer metabolism in full circle. Nat Rev Cancer 13:572

27. Maddocks ODK, Berkers CR, Mason SM, et al (2013) Serine starvation induces stress and p53-dependent metabolic remodelling in cancer cells. Nature 493:542–6

28. Dang C V (2010) Rethinking the Warburg effect with Myc micromanaging glutamine metabolism. Cancer Res 70:859–862

29. Dang L, White DW, Gross S, et al (2009) Cancer-associated IDH1 mutations produce 2-hydroxyglutarate. Nature 462:739

30. De Ruyck JJ, Famerée M, Wouters J, et al (2007) Towards the understanding of the absorption spectra of NAD(P)H/NAD(P)+ as a common indicator of dehydrogenase enzymatic activity. Chem Phys Lett 450:119–122

31. Blacker TS, Marsh RJ, Duchen MR, Bain AJ (2013) Activated barrier crossing dynamics in the non-radiative decay of NADH and NADPH. Chem Phys 422:184–194

32. Patterson GH, Knobel SM, Arkhammar P, et al (2000) Separation of the glucose-stimulated cytoplasmic and mitochondrial NAD(P)H responses in pancreatic islet beta cells. Proc Natl Acad Sci U S A 97:5203–5207

33. Mayevsky A, Chance B (2007) Oxidation-reduction states of NADH in vivo: from

animals to clinical use. Mitochondrion 7:330–9

34. Chance B, Cohen P, Jobsis F, Schoener B (1962) Intracellular oxidation-reduction states in vivo. Science (80-) 137:499–508

35. Duchen MR, Surin A, Jacobson J (2003) Imaging mitochondrial function in intact cells. Methods Enzymol 361:353–389

36. Berezin MY, Achilefu S (2010) Fluorescence lifetime measurements and biological imaging. Chem Rev 110:2641–84

37. Meijers R, Morris RJ, Adolph HW, et al (2001) On the enzymatic activation of NADH. J Biol Chem 276:9316–9321

38. Blacker TS, Mann ZF, Gale JE, et al (2014) Separating NADH and NADPH fluorescence in live cells and tissues using FLIM. Nat Commun 5:3936

39. Schneckenburger H, Koenig K (1992) Fluorescence decay kinetics and imaging of NAD(P)H and flavins as metabolic indicators. Opt Eng 31:1447–1451

40. Paul RJ, Schneckenburger H (1996) Oxygen concentration and the oxidation-reduction state of yeast: Determination of free/bound NADH and flavins by time-resolved spectroscopy. Naturwissenschaften 83:32–35

41. Pradhan A, Pal P, Durocher G, et al (1995) Steady state and time-resolved fluorescence properties of metastatic and non-metastatic malignant cells from different species. J Photochem Photobiol B-Biology 31:101–112

42. Bird DK, Yan L, Vrotsos KM, et al (2005) Metabolic Mapping of MCF10A Human Breast Cells via Multiphoton Fluorescence Lifetime Imaging of the Coenzyme NADH. Cancer Res 65:8766–8773

43. Skala MC, Riching KM, Bird DK, et al (2007) In vivo multiphoton fluorescence lifetime

imaging of protein-bound and free nicotinamide adenine dinucleotide in normal and precancerous epithelia. J Biomed Opt 12:24014

44. McGinty J, Galletly NP, Dunsby C, et al (2010) Wide-field fluorescence lifetime imaging of cancer. Biomed Opt Express 1:627–640

45. Adur J, Pelegati VB, Bianchi M, et al (2013) Multimodal nonlinear optical microscopy used to discriminate human colon cancer. In: Multiphoton Microscopy in the Biomedical Sciences XIII. International Society for Optics and Photonics, p 85881J

46. Rueck AC, Hauser C, Mosch S, Kalinina S (2014) Spectrally resolved fluorescence lifetime imaging to investigate cell metabolism in malignant and nonmalignant oral mucosa cells. J Biomed Opt 19:96005

47. Wang Y, Song C, Wang M, et al (2016) Rapid, label-free, and highly sensitive detection of cervical cancer with fluorescence lifetime imaging microscopy. IEEE J Sel Top Quantum Electron 22:228–234

48. Awasthi K, Moriya D, Nakabayashi T, et al (2016) Sensitive detection of intracellular environment of normal and cancer cells by autofluorescence lifetime imaging. J Photochem Photobiol B Biol 165:256–265

49. Pastore MN, Studier H, Bonder CS, Roberts MS (2017) Non- invasive metabolic imaging of melanoma progression. Exp Dermatol 26:607–614

50. Phillips D, Drake RC, O'Connor D V, Christensen RL (1985) Time correlated single-photon counting (TCSPC) using laser excitation

51. Bain AJ (2015) Multiphoton Processes. In: Photonics. John Wiley & Sons, Inc., Hoboken, NJ, USA, pp 279–320

52. Moulton PF (1986) Spectroscopic and laser characteristics of Ti:Al$_2$O$_3$.JOSAB 3:125–133

53. Helmchen F, Denk W (2005) Deep tissue two-photon microscopy. Nat Methods 2:932–940

54. Schneckenburger H, Wagner M, Weber P, et al (2004) Autofluorescence lifetime imaging of cultivated cells using a UV picosecond laser diode. J Fluoresc 14:649–654

55. Webb RH (1996) Confocal optical microscopy. Reports Prog Phys 59:427

56. Le Grand Y, Leray A, Guilbert T, Odin C (2008) Non-descanned versus descanned epifluorescence collection in two-photon microscopy: Experiments and Monte Carlo simulations. Opt Commun 281:5480–5486

57. Becker W, Bergmann A, Hink MA, et al (2004) Fluorescence lifetime imaging by time-correlated single-photon counting. Microsc Res Tech 63:58–66

58. Becker W, Su B, Holub O (2011) FLIM and FCS detection in laser- scanning microscopes: Increased efficiency by GaAsP hybrid detectors. Microsc Res Tech 74:804–811

59. Becker W, Bergmann A, Biskup C (2007) Multispectral fluorescence lifetime imaging by TCSPC. Microsc Res Tech 70:403–409

60. Zipfel WR, Williams RM, Christie R, et al (2003) Live tissue intrinsic emission microscopy using multiphoton-excited native fluorescence and second harmonic generation. Proc Natl Acad Sci U S A 100:7075–80

61. Moré JJ (1978) The Levenberg-Marquardt algorithm: implementation and theory. In: Numerical analysis. Springer, pp 105–116

62. Wahl P (1979) Analysis of fluorescence anisotropy decays by a least square method. Biophys Chem 10:91–104

63. Moger J, Gribbon P, Sewing A, Winlove CP (2006) The Application of Fluorescence Lifetime Readouts in High-Throughput Screening. J Biomol Screen 11:765–772

64. Tiede LM, Nichols MG (2006) Photobleaching of reduced nicotinamide adenine dinucleotide and the development of highly fluorescent lesions in rat basophilic leukemia cells during multiphoton microscopy. Photochem Photobiol 82:656–664

65. Enderlein J, Erdmann R (1997) Fast fitting of multi-exponential decay curves. Opt Commun 134:371–378

66. Laurence TA, Chromy BA (2010) Efficient maximum likelihood estimator fitting of histograms. Nat Methods 7:338

67. Turton DA, Reid GD, Beddard GS (2003) Accurate analysis of fluorescence decays from single molecules in photon counting experiments. Anal Chem 75:4182–4187

68. Maus M, Cotlet M, Hofkens J, et al (2001) An experimental comparison of the maximum likelihood estimation and nonlinear least-squares fluorescence lifetime analysis of single molecules. Anal Chem 73:2078–2086

69. Bajzer Ž, Therneau TM, Sharp JC, Prendergast FG (1991) Maximum likelihood method for the analysis of time-resolved fluorescence decay curves. Eur Biophys J 20:247–262

70. Warren SC, Margineanu A, Alibhai D, et al (2013) Rapid global fitting of large fluorescence lifetime imaging microscopy datasets. PLoS One 8:e70687

71. Livesey AK, Brochon JC (1987) Analyzing the distribution of decay constants in pulse-fluorimetry using the maximum entropy method. Biophys J 52:693–706

72. Brochon J-C (1994) Maximum entropy method of data analysis in time-resolved spectroscopy. In: Methods in enzymology. Elsevier, pp 262–311

73. Rowley MI, Coolen ACC, Vojnovic B, Barber PR (2016) Robust Bayesian fluorescence lifetime estimation, decay model selection and instrument response determination for low-intensity FLIM imaging. PLoS One 11:e0158404

74. Rowley MI, Barber PR, Coolen ACC, Vojnovic B (2011) Bayesian analysis of fluorescence lifetime imaging data. In: Multiphoton Microscopy in the Biomedical Sciences XI. International Society for Optics and Photonics, p 790325

75. O'Shea P (2012) Future medicine shaped by an interdisciplinary new biology. Lancet 379:1544–50

76. Digman MA, Caiolfa VR, Zamai M, Gratton E (2008) The phasor approach to fluorescence lifetime imaging analysis. Biophys J 94:L14-6

77. Plotegher N, Stringari C, Jahid S, et al (2015) NADH fluorescence lifetime is an endogenous reporter of α-synuclein aggregation in live cells. FASEB J 29:2484–94

78. Stringari C, Cinquin A, Cinquin O, et al (2011) Phasor approach to fluorescence lifetime microscopy distinguishes different metabolic states of germ cells in a live tissue. Proc Natl Acad Sci 108:13582–13587

79. Stringari C, Edwards RA, Pate KT, et al (2012) Metabolic trajectory of cellular differentiation in small intestine by Phasor Fluorescence Lifetime Microscopy of NADH. Sci Rep 2:

80. Talbot CB, Patalay R, Munro I, et al (2011) Application of ultrafast gold luminescence to measuring the instrument response function for multispectral multiphoton fluorescence lifetime imaging. Opt Express 19:13848–61

81. Czochralska B, Lindqvist L (1983) Diphotonic one-electron oxidation of NADH on laser excitation at 353 nm. Chem Phys Lett 101:297–299

82. Walsh AJ, Cook RS, Sanders ME, et al (2014) Quantitative optical imaging of primary tumor organoid metabolism predicts drug response in breast cancer. Cancer Res 74:5184–5194

83. Kawano H, Nabekawa Y, Suda A, et al (2003) Attenuation of photobleaching in two-photon excitation fluorescence from green fluorescent protein with shaped excitation pulses. Biochem Biophys Res Commun 311:592–596

84. Salthammer T (1992) Numerical simulation of pile-up distorted time-correlated single photon counting (TCSPC) data. J Fluoresc 2:23–27

85. Tosatto A, Sommaggio R, Kummerow C, et al (2016) The mitochondrial calcium uniporter regulates breast cancer progression via HIF-1α. EMBO Mol Med 8:569–85

86. Baffou G, Rigneault H, Marguet D, Jullien L (2014) A critique of methods for temperature imaging in single cells. Nat Methods 11:899

87. Cracan V, Titov D V, Shen H, et al (2017) A genetically encoded tool for manipulation of NADP+/NADPH in living cells. Nat Chem Biol 13:1088

88. Guo H-W, Yu J-S, Hsu S-H, et al (2015) Correlation of NADH fluorescence lifetime and oxidative phosphorylation metabolism in the osteogenic differentiation of human mesenchymal stem cell. J Biomed Opt 20:17004

89. Schaefer PM, Hilpert D, Niederschweiberer M, et al (2017) Mitochondrial matrix pH as a decisive factor in neurometabolic imaging. Neurophotonics 4:45004

90. Sun Y, Phipps J, Elson DS, et al (2009) Fluorescence lifetime imaging microscopy: in vivo application to diagnosis of oral carcinoma. Opt Lett 34:2081–2083

91. De Beule PA, Dunsby C, Galletly NP, et al (2007) A hyperspectral fluorescence lifetime probe for skin cancer diagnosis. Rev Sci Instrum 78:123101

92. Butte P V, Pikul BK, Hever A, et al (2005) Diagnosis of meningioma by time-resolved fluorescence spectroscopy. J Biomed Opt 10:64026–64029
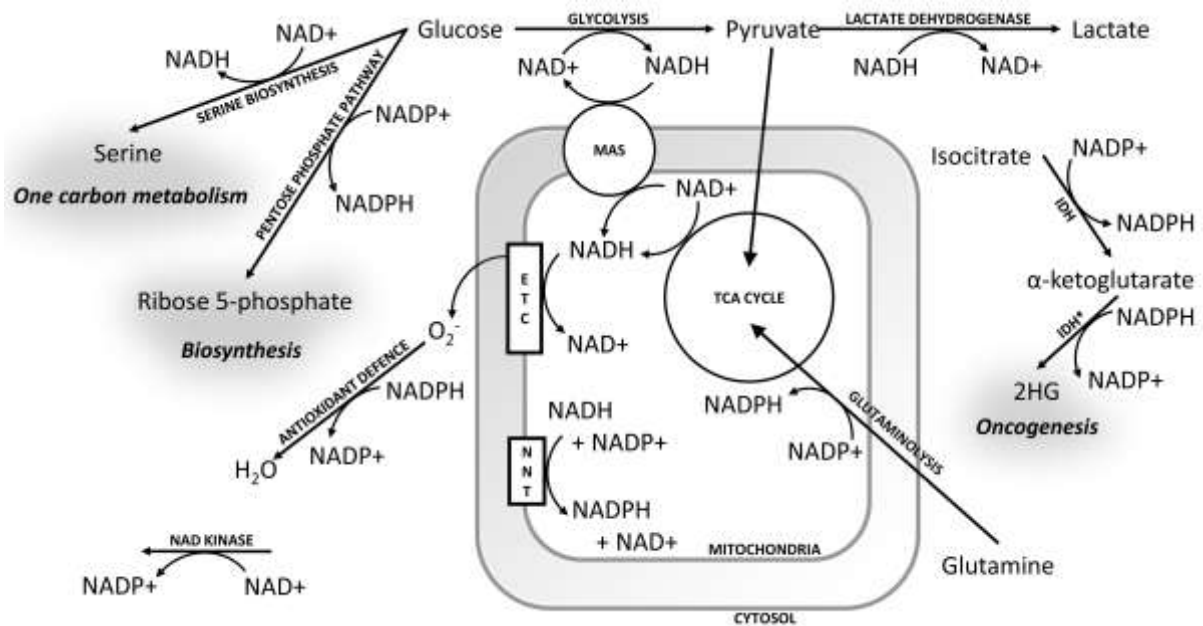
Figure 1: NADH and NADPH play a role in a large number of the metabolic pathways known to be altered in cancer cells. NADH is involved in the pathways whose relative activities are altered by the Warburg effect; cytosolic glycolysis and mitochondrial energy metabolism, linking the tricarboxylic acid (TCA) cycle and electron transport chain (ETC). NADH is also produced during serine biosynthesis, a key feature of p53 deficient tumours. Meanwhile, NADPH is involved in the biosynthetic pathways required for cell proliferation. In the mitochondria, NADPH is primarily produced by the nicotinamide nucleotide transhydrogenase (NNT). In the cytosol, both the pentose phosphate pathway and isocitrate dehydrogenase (IDH) contribute. IDH mutation is a known oncogenic transformation, causing oxidation of NADPH and production of 2-hydroxyglutarate, an oncometabolite.
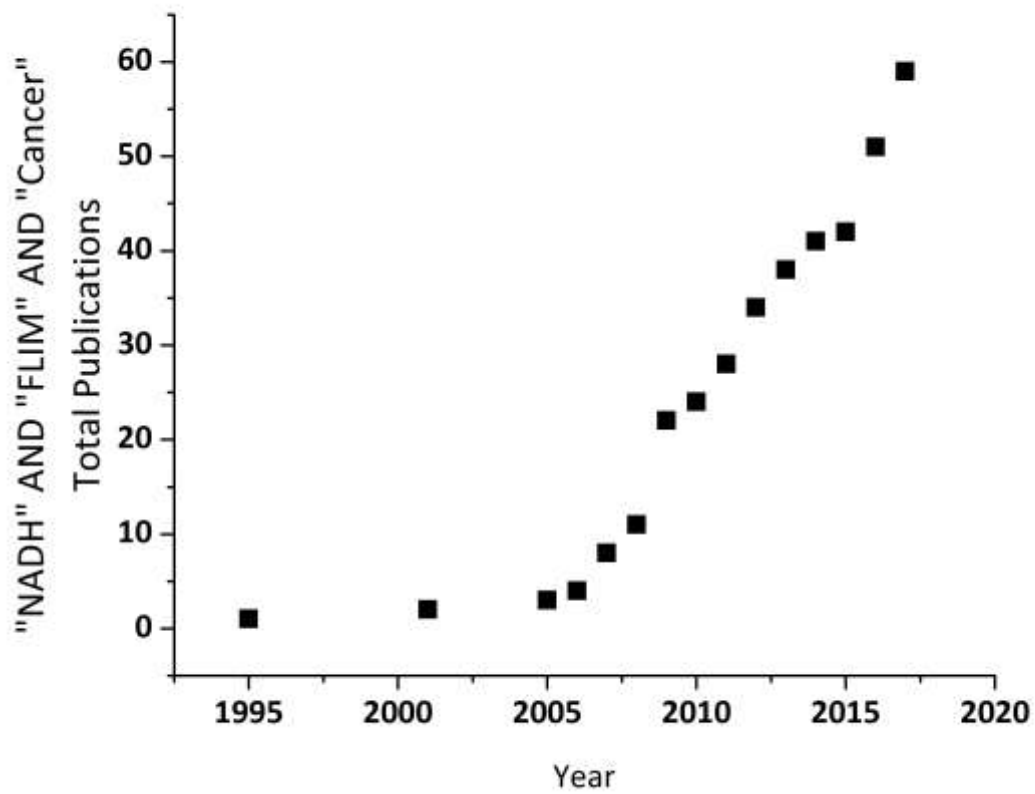
Figure 2: Following commercialisation of time-resolved fluorescence imaging technology in the early 2000's, the number of FLIM studies of NADH in cancer has increased approximately linearly since 2005 (Scopus).
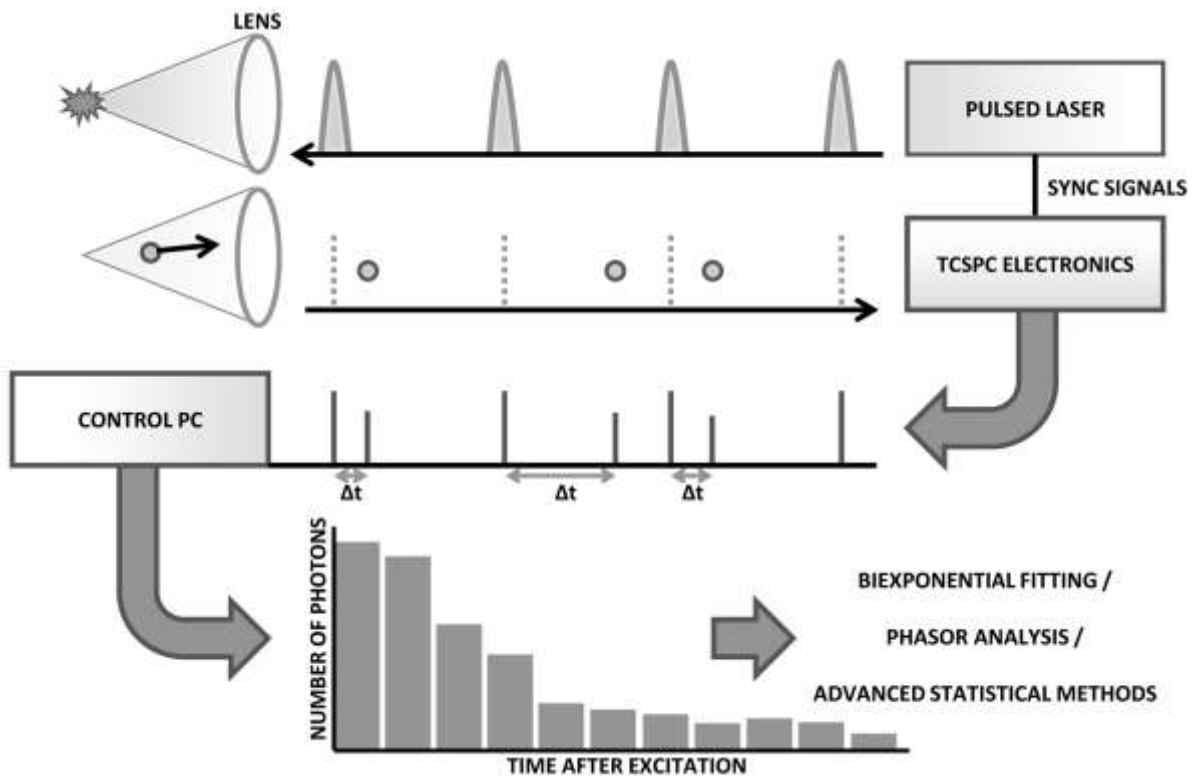
Figure 3: A schematic overview of the time-correlated single photon counting (TCSPC) method. Light from a pulsed laser source is focused onto a sample. Fluorescence photons emitted by the target molecules are registered by a detector. Electronics in a PC measure the time delay between the incident pulse and the fluorescence emission. The excitation-emission delay times are recorded in a histogram. This data is then analysed to extract the fluorescence decay dynamics. FLIM combines this approach with the x-y coordinates provided by microscope scan heads to build up fluorescence decay histograms at every pixel of an image.